PHYSICAL REVIEW B **109**, 155153 (2024)

Switchable in-plane anomalous Hall effect by magnetization orientation in monolayer $Mn_3Si_2Te_6$

Ding Li,[1,2] Maoyuan Wang,[3,*] Dengfeng Li,[4,5] and Jianhui Zhou[1,†]
[1]*Anhui Key Laboratory of Low-Energy Quantum Materials and Devices, High Magnetic Field Laboratory, HFIPS, Chinese Academy of Sciences, Hefei, Anhui 230031, China*
[2]*Department of Physics, University of Science and Technology of China, Hefei 230026, People's Republic of China*
[3]*Department of Physics, Xiamen University, Xiamen 361005, China*
[4]*School of Science, Chongqing University of Posts and Telecommunications, Chongqing 400065, China*
[5]*Institute for Advanced Sciences, Chongqing University of Posts and Telecommunications, Chongqing 400065, China*

(Received 2 September 2023; revised 30 January 2024; accepted 1 April 2024; published 18 April 2024)

In-plane anomalous Hall effect (IPAHE) is an unconventional anomalous Hall effect (AHE) where the Hall current flows in the plane spanned by the magnetization or magnetic field and the electric field. Here, we predict a stable two-dimensional ferromagnetic monolayer $Mn_3Si_2Te_6$ with collinear ordering of Mn moments in the basal plane. Moreover, we reveal that monolayer $Mn_3Si_2Te_6$ possesses a substantial periodic IPAHE due to the threefold rotational symmetry, which can be switched by changing the magnetization orientation by external magnetic fields. In addition, we briefly discuss the impacts of moderate strains on the electronic states and the AHE, which lead to a near quantized Hall conductivity. Our work provides a potential platform for realizing a sizable and controllable IPAHE that greatly facilitates the application of energy-efficient spintronic devices.

DOI: 10.1103/PhysRevB.109.155153

I. INTRODUCTION

The conventional anamalous Hall effect (AHE) with the orthogonal magnetization, electric field, and Hall current in ferromagnetic (FM) materials could be crucial in understanding dissipationless quantum phenomena [1,2] and realizing low-power spintronic devices [3–6]. In magnetic materials, the Onsager relation allows the unconventional AHE with the planar configuration among the magnetization/magnetic field, the Hall current, and the electric field named the in-plane AHE (IPAHE) [7]. It originates from the Berry curvature of electrons and is in contrast to the conventional planar Hall effect that has the essential nature of anisotropic magnetoresistance [8–12]. Recently, the IPAHE and its quantized counterpart have attracted significant attention and been theoretically investigated in various quantum materials, such as thin films of magnetic/nonmagnetic topological insulators, graphenelike systems, monolayer transitional-metal oxides, and van der Waals heterostructures [13–25]. Remarkably, the IPAHE has been reported experimentally in heterodimensional VS_2-VS superlattice [25,26]. However, realistic magnetic materials with easily tunable in-plane magnetization orientation that harbor IPAHE are still challenging.

Recently, a colossal angular-dependent magnetoresistance has been reported in $Mn_3Si_2Te_6$ single crystals [27,28], in which a seven-order-of-magnitude reduction occurred in *ab* plane resistivity and was attributed to the metal-insulator transition driven by lifting of the topological band degeneracy [27] or the first-order "melting transition" driven by chiral orbital currents [29]. Moreover, $Mn_3Si_2Te_6$ exhibits a variety of intriguing quantum phenomena [30–41], such as polaronic transport and a sizable anomalous Nernst signal. Notably, a quasi-two-dimensional $Mn_3Si_2Te_6$ nanosheet for ultrafast photonics has been obtained by a mechanical exfoliation procedure [42], enabling us to investigate novel quantum states in few layers and monolayers of $Mn_3Si_2Te_6$. Furthermore, $Mn_3Si_2Te_6$ exhibits typical characteristics of soft magnetic materials with rapid response to in-plane magnetic fields [30]. Thus, monolayer $Mn_3Si_2Te_6$ provides a practical material platform for the interplay between electronic topology, orbital physics, and magnetism.

In this work, we systematically investigate the magnetism, the electronic structure, and the intrinsic AHE of monolayer $Mn_3Si_2Te_6$. We find that monolayer $Mn_3Si_2Te_6$ has no imaginary frequency in the phonon spectrum and displays unusual in-plane magnetization with a tiny planar magnetic anisotropy energy (MAE). Notably, a significant sixfold AHE is found in monolayer $Mn_3Si_2Te_6$ and can be controllable by manipulating the magnetization orientation. Moreover, the strain effects on the electronic states and the AHE are also explored.

II. STRUCTURE PROPERTIES

The ferrimagnetic compound $Mn_3Si_2Te_6$ crystalizes in a layered structure with the space group $P\bar{3}1c$ (No. 163) [30,43]. The crystal structure of monolayer $Mn_3Si_2Te_6$ has the space group $P\bar{3}1m$ (No. 162) that only contains the rotational part of $P\bar{3}1c$, as shown in Fig. 1(a). Note that both $P\bar{3}1m$ and $P\bar{3}1c$ possess the same point group D_{3d}. Each Mn atom is coordinated by six Te atoms forming a distorted octahedral

---

[*] mywang@xmu.edu.cn

[†] jhzhou@hmfl.ac.cn

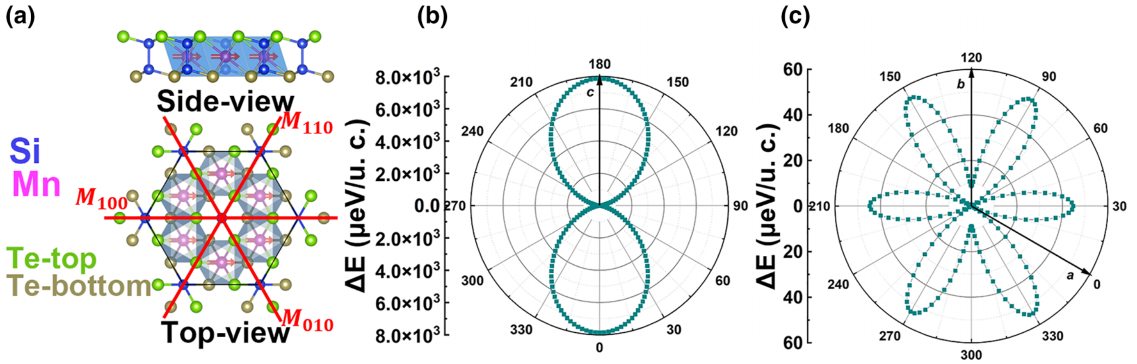

FIG. 1. (a) The top and side views of monolayer $Mn_3Si_2Te_6$, where Mn, Si, Te-top, and Te-bottom are represented by pink, blue, green, and brown balls, respectively. The nattier blue face represents the distorted Te octahedral. The energy variation depends on (b) the polar angle of magnetization in the basal plane and (c) the plane perpendicular to the *a* axis of monolayer $Mn_3Si_2Te_6$.

crystal field [44]. The Mn atoms form a simple hexagonal lattice at the 2c Wyckoff position. Monolayer $Mn_3Si_2Te_6$ includes five atomic layers and ten atoms per primitive hexagonal unit cell, with the Si atom being surrounded by six Te atoms. It is noteworthy that the Te atoms are not on the same plane and form the low-buckled structure, which breaks the out-of-plane mirror reflection and would be crucial to realizing novel topological quantum states [45,46]. The crystal structure of monolayer $Mn_3Si_2Te_6$ has the point group D_{3d} with three mirror symmetries labeled $\mathcal{M}_{[0\,1\,0]}$, $\mathcal{M}_{[1\,0\,0]}$, and $\mathcal{M}_{[1\,1\,0]}$, as illustrated in Fig. 1(a). When the moments are rotated in the x-y plane, only the mirror normal to the magnetization direction [i.e., $\phi = (2n+1)\pi/6$, with $n = 0, 1, \ldots, 5$] can be preserved (because the magnetization is a pseudovector). For instance, as shown in Fig. 2(d), if the magnetization direction is along $\phi = \pi/6$, the mirror $\mathcal{M}_{[0\,1\,0]}$ is persevered. As a result, this system has three different magnetic space groups depending on the orientation of the moments with respect to ϕ. It has magnetic space groups $C2'/m'$ and $C2/m$ at $\phi = 2n\pi/6$ and $\phi = (2n+1)\pi/6$, respectively. For any other general orientations, it has the magnetic space group $P-1$ with only two symmetry operations, i.e., E (identity) and P (inversion). The lattice constants are listed in Table I. The structural stability is examined by the phonon spectra calculations (see computational details in Appendix A). There are no evident soft modes at finite q in the calculated

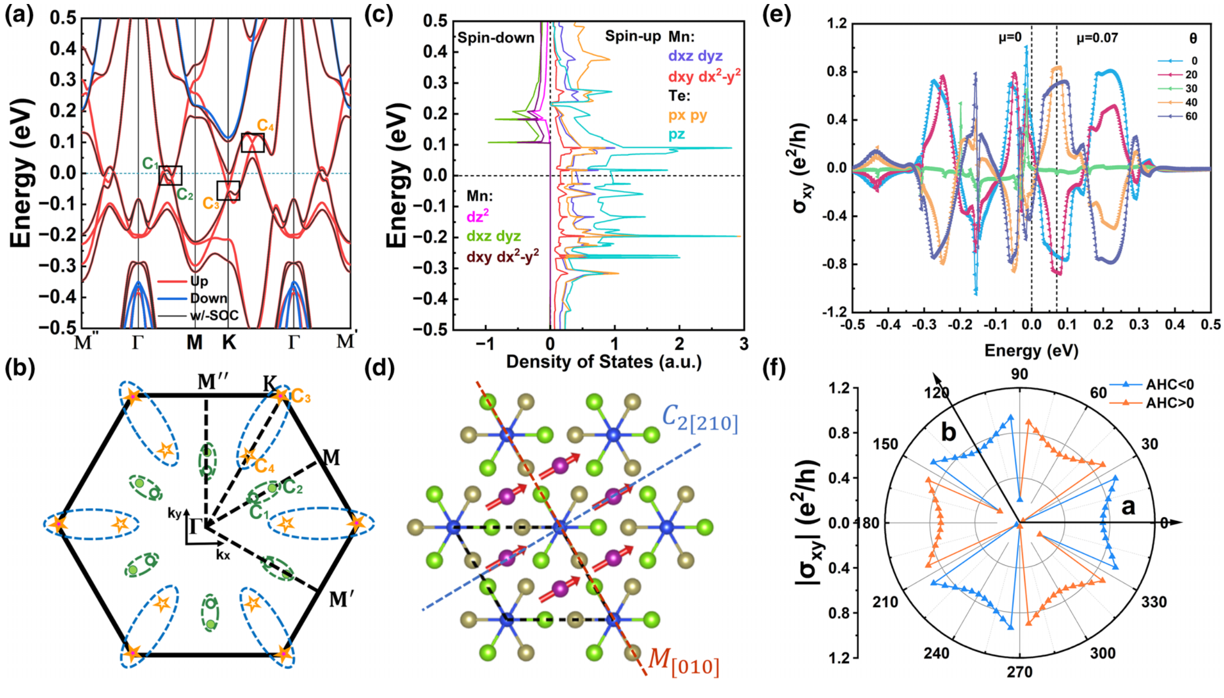

FIG. 2. (a) Band structure of monolayer $Mn_3Si_2Te_6$ with and without SOC. $\mathcal{C}_n$ labels the degenerate points. (b) The distributions of degenerate points in the first BZ. (c) The dominant components of PDOS of monolayer $Mn_3Si_2Te_6$ without SOC. (d) The illustration of $\mathcal{C}_2$ and mirror $\mathcal{M}$ symmetry at $\phi = \pi/6$. (e) The calculated AHC vs Fermi energy with ϕ at 0°, 20°, 30°, 40°, and 60°. (f) The AHC vs different in-plane magnetization with a given Fermi energy of 0.07 eV. The values represent the magnitudes of AHCs, and the blue and orange colors represent negative and positive AHCs, respectively.

TABLE I. Lattice constants, thickness, bond angle of Te-Mn-Te, and total energy E (meV) for Néel, stripe, and zigzag in-plane AFM configurations with the Néel vector in the x direction per unit cell relative to the FM ground state.

	a (Å)	d (Å)	θ (°)	Néel x	Stripe x	Zigzag x
$Mn_3Si_2Te_6$	6.856	3.559	86.2	154.6	23.3	14.2

phonon spectrum, probably implying the mechanical stability of monolayer $Mn_3Si_2Te_6$, as shown in Fig. 5. The ultrathin $Mn_3Si_2Te_6$ nanoflakes obtained by using a simple mechanical exfoliation procedure in Ref. [42] indicated that monolayer $Mn_3Si_2Te_6$ could exist stably and be prepared by the delicate mechanical exfoliation or by growth via the molecular beam epitaxy technique.

III. MAGNETIC PROPERTIES

In order to uncover the nature of the magnetic ground state of monolayer $Mn_3Si_2Te_6$, we performed the electronic structure calculations by considering typical magnetic configurations of Mn spin moments (see Appendix B) [24,47], i.e., FM, (ii) Néel antiferromagnetic (AFM), (iii) stripe AFM, and (iv) zigzag AFM aligned in three directions. Table I lists the AFM energy of some in-plane AFM configurations with the Néel vector in the x direction relative to the FM ground state in units of meV. The total energies of these configurations aligned in three directions listed in Table III indicate that the FM state is preferred in monolayer $Mn_3Si_2Te_6$, illustrated in Fig. 1(a). Noted that the origin of the FM order in monolayer $Mn_3Si_2Te_6$ may share the same mechanism of Ruderman-Kittel-Kasuya-Yosida interaction mediated by the itinerant carriers as the monolayer $MnSiTe_3$ with out-of-plane FM order [47]. For the FM state, the calculated local magnetic moments of Mn are about 3.816 μ_B per Mn atom, close to the experimental value in the single crystals [30].

We further calculate the MAE to obtain the easy magnetization direction. The MAEs in different directions relative to the z axis are shown in Fig. 1(b). It can be seen that the magnetization is predominantly oriented in the basal plane with strong anisotropy, and the dipolar energy is about 7.87 meV. In the basal plane of monolayer $Mn_3Si_2Te_6$, the angular dependence of the total energy [shown in Fig. 1(c)] indicates that the magnetization lies in the a axis or the 60° direction, with a slight degree of in-plane magnetic anisotropy that produces only 54 μeV of dipolar energy. The large MAE of out-of-plane magnetization and the negligible difference in in-plane magnetization imply the feasible manipulation of in-plane magnetization orientation.

TABLE II. Constraint on the IPAHE under symmetry operations. The label Y (N) denotes symmetry allowed (forbidden).

Sym. operator	$\mathcal{M}_{x/y}$	$\mathcal{M}_z$	$\mathcal{T}\mathcal{M}_{x/y}$	$\mathcal{T}\mathcal{M}_z$	$\mathcal{C}_{3z}$	$\mathcal{T}\mathcal{C}_{3z}$	$\mathcal{C}_2$	$\mathcal{T}\mathcal{C}_2$
$\sigma_{\rm Hall}$	N	Y	Y	N	Y	N	N	Y

TABLE III. Total energy E (meV) for FM, Néel, stripe, and zigzag antiferromagnetic configurations with the Néel vector in the x direction per unit cell, where zero is set as the energy of the FM configuration with spin in the x direction.

	FM	Néel	Stripe	Zigzag
Spin z	18.3	173.7	42.5	304.2
Spin x	0	183.0	32.5	297.3
Spin y	0.0	184.4	34.7	263.4

IV. ELECTRONIC STRUCTURE

Figure 2(a) shows the band structures and density of states (DOS) of the magnetic ground state of monolayer $Mn_3Si_2Te_6$ with and without spin-orbit coupling (SOC). One can see that the bands in the spin-up channel [48] are insulating with a gap of 0.46 eV, whereas only the spin-down channel crosses the Fermi level, thus monolayer $Mn_3Si_2Te_6$ has a half-metallic character. For the spin-down states, we find the linear band crossings near the Fermi level labeled by $\mathcal{C}_1$ to $\mathcal{C}_4$ in the first Brillouin zone (BZ) as shown in Fig. 2(b). Meanwhile, we plot the dominant components of partial density of states without SOC around the Fermi energy [shown in Fig. 2(c)]. It is clear that the DOS around Fermi energy are dominated by Mn d_{xz}, d_{yz}, d_{xy}, and $d_{x^2-y^2}$ orbitals and Te $p_{x,y,z}$ orbitals in the spin-up channel. We also identify several sharp peaks that correspond to van Hove singularities, such as the one slightly above the Fermi energy and the one from the nearly flat band near the M point (about −0.3 eV). After taking account of the SOC, the band anticrossings open small gaps, which could host nonzero Berry curvature, implying a finite AHE in monolayer $Mn_3Si_2Te_6$.

It should be noted that there are three inequivalent Γ-M lines, i.e., Γ-M, Γ-M′, and Γ-M″, as shown in Fig. 7. For example, when the magnetization direction is along $\phi = \pi/6$, the $\mathcal{C}_2$ operation makes Γ-M′ equivalent to Γ-M″. Meanwhile, the mirror $\mathcal{M}_{[1\,0\,0]}$ operation makes Γ-M equivalent to Γ-M′ for the magnetization direction being along $\phi = \pi/2$. We also calculated the energy dispersions along the M″-Γ-M-K-Γ-M′ path for six representative orientations of the magnetic moments, as shown in Fig. 2(b) and Appendix B. The calculated band dispersions are consistent with the symmetry analysis. Note that the similarity of the energy dispersions for inequivalent Γ-M lines might come from the small planar magnetic anisotropy energy that does cause dramatic change of energy bands except for the parts near the Fermi energy.

In fact, the two bands are degenerate protected by $\mathcal{M}_{[0\,1\,0]}$ for $\phi = (2n+1)\pi/6$, but become split for other orientations. The above discussion pointed out that this material has a type-I magnetic space group, $C2/m$, at $\phi = (2n+1)\pi/6$. Based on the group representation theory, the wave-vector group along Γ-M only have one-dimensional irreducible representations [44]. Meanwhile, the two bands near the crossing point belong to different irreps LD_1 and LD_2. Therefore, the crossing states transform according to different irreducible representations of the wave-vector group of the high-symmetry path Γ-M. Their hybridization is prevented and a crossing at this point of intersection is symmetry protected.

V. MAGNETIZATION-ORIENTATION-DEPENDENT ANOMALOUS HALL EFFECT

Symmetry analysis provides a useful tool to understand various physical properties of solids, such as electric conductivity tensors [49,50]. Recent work further reveals that the mirror symmetry $\mathcal{M}_\gamma$, the rotational symmetry $\mathcal{C}_{n\gamma}$, and their combination with time-reversal symmetry $\mathcal{T}$ could effectively determine the IPAHE in magnetic materials [25]. For monolayer $Mn_3Si_2Te_6$, the point group D_{3d} contains three twofold rotations $\mathcal{C}_2$ in the basal plane, two threefold rotations $\mathcal{C}_3$ perpendicular to the basal plane, and the combined symmetry with spatial inversion. For example, the two-dimensional (2D) Hall effect is expressed as $j_y = \sigma_{xy}E_x$. Since the electric field is even and the electric current is odd under the mirror reflection about the y plane ($\mathcal{M}_x$), the Hall response equation becomes $j_y = -\sigma_{xy}E_x$. Consequently, σ_{xy} should vanish if the $\mathcal{M}_x$ invariant is present. It can also be seen from the transforming of Berry curvature under the mirror operation. The mirror operation $\mathcal{M}_x$ acts on the Berry curvature Ω_{xy} as $\mathcal{M}_x\Omega_{xy}(\boldsymbol{k}) = -\Omega_{xy}(-k_x, k_y)$. For a system respecting $\mathcal{M}_x$, it leads to $\mathcal{M}_x\Omega_{xy}(\boldsymbol{k}) = -\Omega_{xy}(-k_x, k_y) = \Omega_{xy}(k_x, k_y)$. Because the Berry curvature is an odd function of k_x, the integration of Berry curvature over the whole Brillouin zone vanishes. It is known that, the in-plane magnetization is perpendicular to the mirror plane, and the corresponding mirror symmetry is preserved. Thus, we need to break all in-plane mirror symmetries to realize a nonzero IPAHE as well as its quantized version. For this material, the detailed constraints on the IPAHE under symmetry operations are summarized in Table II.

Figure 2(d) shows one special orientation of magnetization ($\phi = 30^\circ$) within the basal plane, where ϕ is the angle between magnetization and the x axis. In this situation, the magnetization is perpendicular to the mirror plane $\mathcal{M}_{[0\,1\,0]}$, and the AHE vanishes due to the related mirror symmetry. This symmetry analysis can be applicable to the other two mirror planes that can be connected by the $\mathcal{C}_{3z}$ rotational operation.

It is known that, for 2D materials, the anomalous Hall conductivity (AHC) can be evaluated by integrating the Berry curvature of electrons over the BZ [2]. Figure 2(e) shows the calculated AHC relative to the Fermi level along different magnetization orientations. One finds that, for the magnetization aligned with the 30° and 90° directions and the electric current along the x axis, the AHCs vanish at the entire energy range [51]. The AHCs in the directions 20° and 40° have almost the same magnitudes but opposite signs. The magnitudes of AHCs are sensitive to the Fermi energy, which can be enhanced by shifting the chemical potential [e.g., $\sigma_{xy} = -0.86$ (e^2/h) at $\mu = 0.07$ eV].

Figure 2(f) shows the calculated AHC as a function of the magnetization direction ϕ for a given chemical potential at $\mu = 0.07$ eV. As discussed above, the symmetry restrictions of monolayer $Mn_3Si_2Te_6$ force $\sigma_{xy}(\phi_n) = 0$, where $\phi_n = (2n+1)\pi/6$, with $n = 0$, 1, 2, 3, 4, and 5. We also found the switching of $\sigma_{xy}(\phi)$ on both sides of ϕ_n, which means that one can change the ϕ slightly around ϕ_n and reverse the sign of the AHC. In particular, the tiny MAE in the basal plane allows an easy switching of the AHE via a small external magnetic field to change the direction of magnetization. The AHC with magnetization $\boldsymbol{M}$ is marked as $\sigma_{xy}(\boldsymbol{M})$, where the angle of $\boldsymbol{M}$ to the crystallographic a axis is located in the region of blue in Fig. 2(f). Next, for the opposite magnetization $-\boldsymbol{M}$, the corresponding AHC is $\sigma_{xy}(-\boldsymbol{M})$. The dissipationless nature of the AHE implies that the Hall conductivity is odd in magnetization or magnetic field, that is, $\sigma_{xy}(\boldsymbol{M}) = -\sigma_{xy}(-\boldsymbol{M})$ [7]. Due to the $\mathcal{C}_{3z}$ rotational symmetry and the time-reversal symmetry, one can reach the periodic AHE with ϕ that disappears at special directions ϕ_n. These distinctive features of the IPAHE here could be detected in the four- or six-Hall setup in conventional transport experiments.

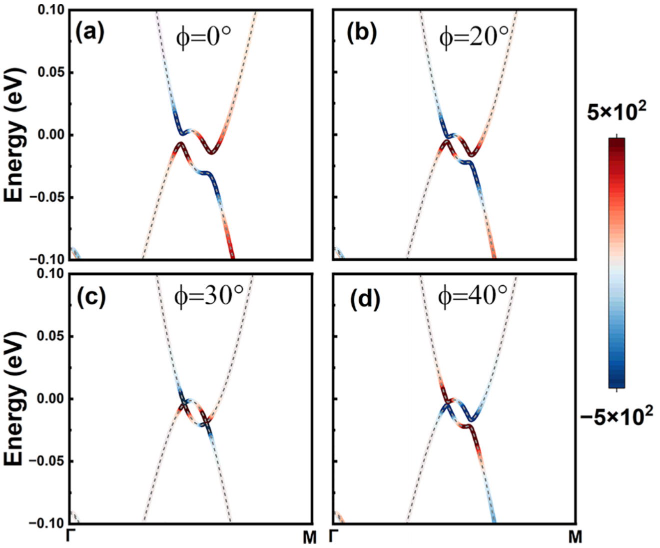

FIG. 3. Band-resolved Berry curvature distribution for some selected magnetization orientations in 0° (a), 20° (b), 30° (c), and 40° (d). In the direction of $\phi = 30^\circ$, the closure of the energy gaps in the Γ-M path leads to AHC vanishing. As the direction changes from 30° to 0°, the gaps increase gradually, and the AHC achieves its maximal value near 30°. For the directions $\phi = 20^\circ$ and $\phi = 40^\circ$, the Berry curvatures are opposite.

In order to better understand the AHE, we calculate the obtained band-resolved Berry curvature distribution and depict the results in Fig. 3 (the whole high-symmetry path is shown in Fig. 8). It is clear that the splitting of the doubly degenerate bands generates a nonzero Berry curvature near the gap opening area (hot spots), leading to a finite AHE at $\phi = 0^\circ$. The AHC disappears at $\phi = 30^\circ$ due to the opposite Berry curvature contributed by the up and down bands near the crossing point, which is consistent with the symmetry constraint. In addition, for two angles ϕ_1 and ϕ_2 that are symmetric relative to the critical angles (e.g., $\phi_1 = 20^\circ$ and $\phi_2 = 40^\circ$) and break the mirror symmetry, both have the same magnitude of Berry curvature with opposite signs resulting from the opposite-sign Rashba SOC mass term, leading to the opposite AHC. It can be understood by the band inversion mechanism associated with a sign reversal of energy gaps, such as near the $\mathcal{C}_1$ and $\mathcal{C}_2$ points [52]. In addition, the Berry curvature dipole and the resulting nonlinear Hall effect are allowed in $Mn_3Si_2Te_6$ [53–55] and deserve further discussions.

Pressure or strain serves as a powerful control knob for tuning the physical properties of solids via altering the crystal constants. Stimulated by recent experiments showing that

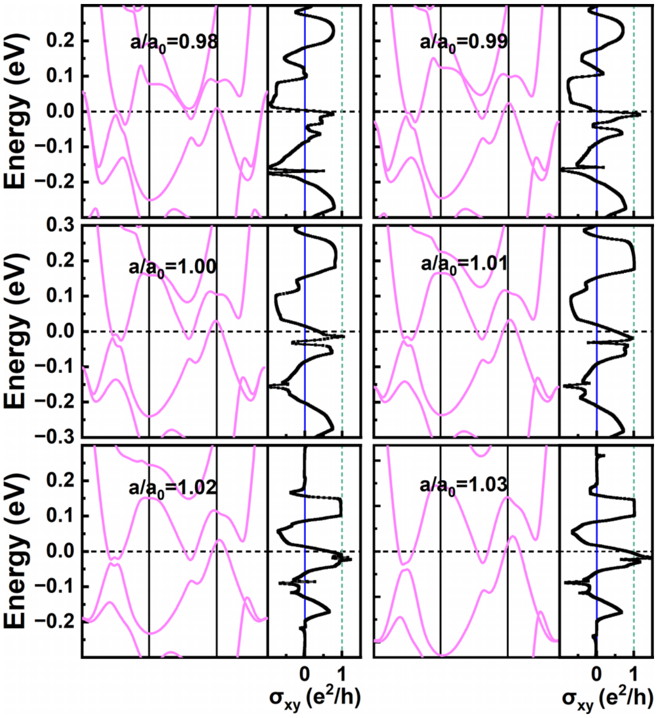

FIG. 4. The calculated energy bands with magnetization orientations at $\phi = 0^\circ$ along the Γ-M-K-Γ line and the AHE for selected in-plane strains (a) $a/a_0 = 0.98$, (b) $a/a_0 = 0.99$, (c) $a/a_0 = 1.01$, and (d) $a/a_0 = 1.02$. a/a_0 represents modification of the lattice constant relative to the initial one a_0.

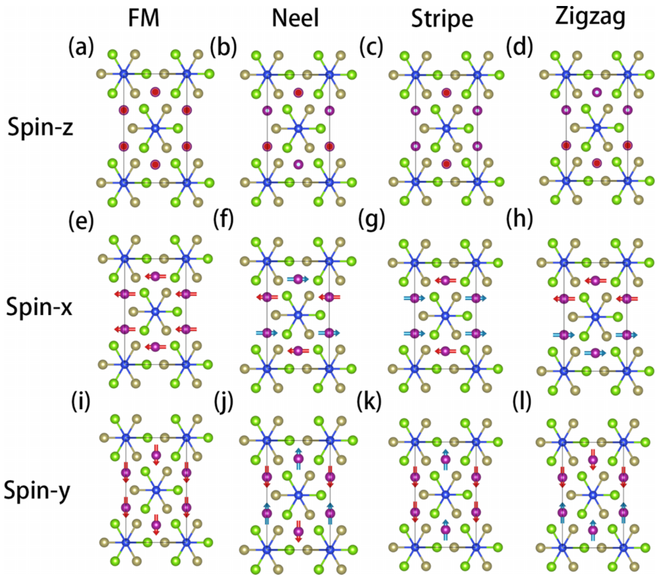

FIG. 6. FM and three AFM configurations with the Néel vector in x, y, and z directions corresponding to Table III.

pressure could dramatically modify the electronic states and the novel colossal magnetoresistance in bulk $Mn_3Si_2Te_6$ [34], we thus would like to investigate the strain effect on the electronic states and the corresponding AHE in monolayer $Mn_3Si_2Te_6$ and present the calculated results in Fig. 4. One can see that the energy bands near the Fermi level hosting the Berry curvature hot spots almost remain unchanged. Interestingly, the moderate tensional strain ($a/a_0 = 1.02$) greatly enlarges the band separation (0.15–0.20 eV) along the M-K direction, leading to a near quantized Hall conductivity [Fig. 4(d)], which may be observed through electric gating or doping. In comparison, we also calculate the behaviors of energy bands and the AHE versus c-axis compressible or tensile strains in $Mn_3Si_2Te_6$ crystal, as shown in Figs. 9 and 10. We find a pressure-induced semiconductor-metal transition around ($c/c_0 = 1.02$), which is consistent with recent experiments [34]. Second, the large IPAHE σ_{xy} and

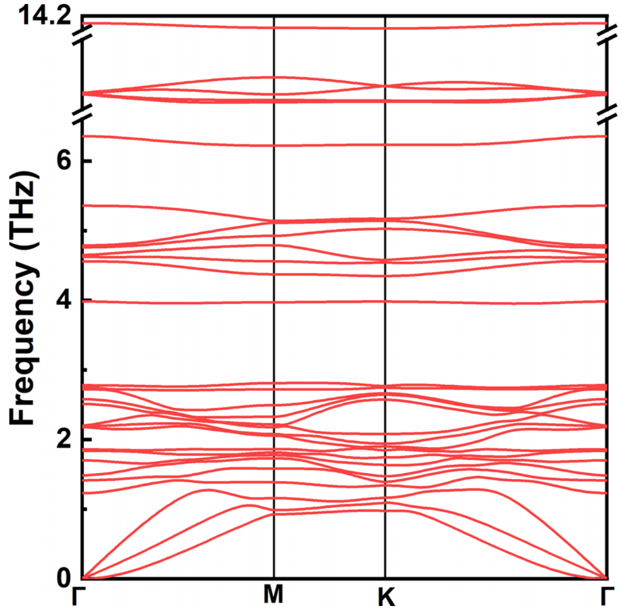

FIG. 5. The calculated phonon dispersion of monolayer $Mn_3Si_2Te_6$.

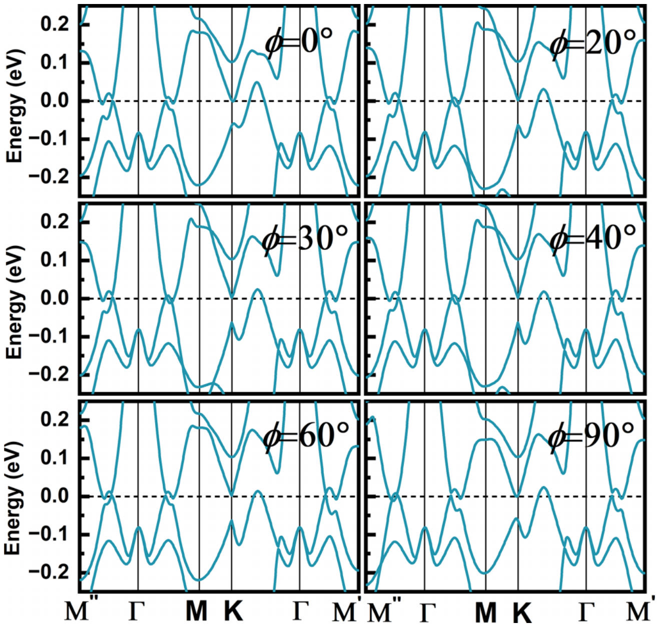

FIG. 7. The calculated energy band of six representative orientations of the moments.

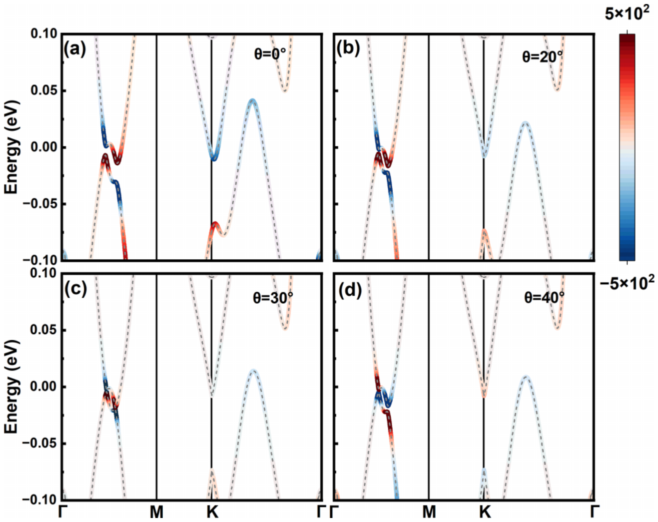

FIG. 8. Band-resolved Berry curvature distribution for some selected magnetization orientations in 0° (a), 20° (b), 30° (c), and 40° (d).

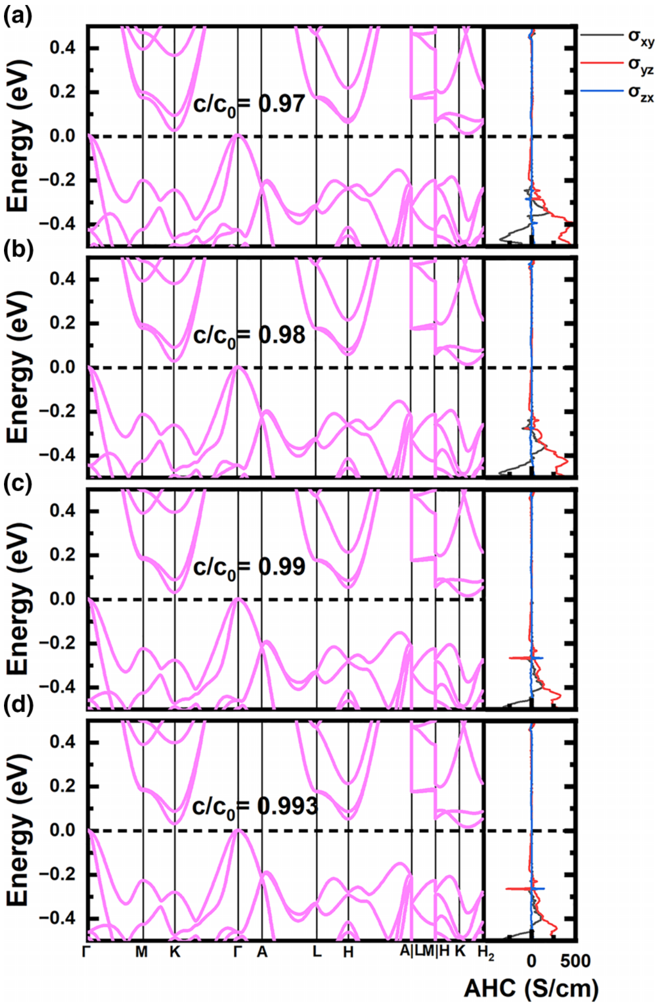

FIG. 9. The AHC at different compressible strains along the c axis of bulk $Mn_3Si_2Te_6$, where c/c_0 represents the ratio between the strained lattice parameter c and the initial value.

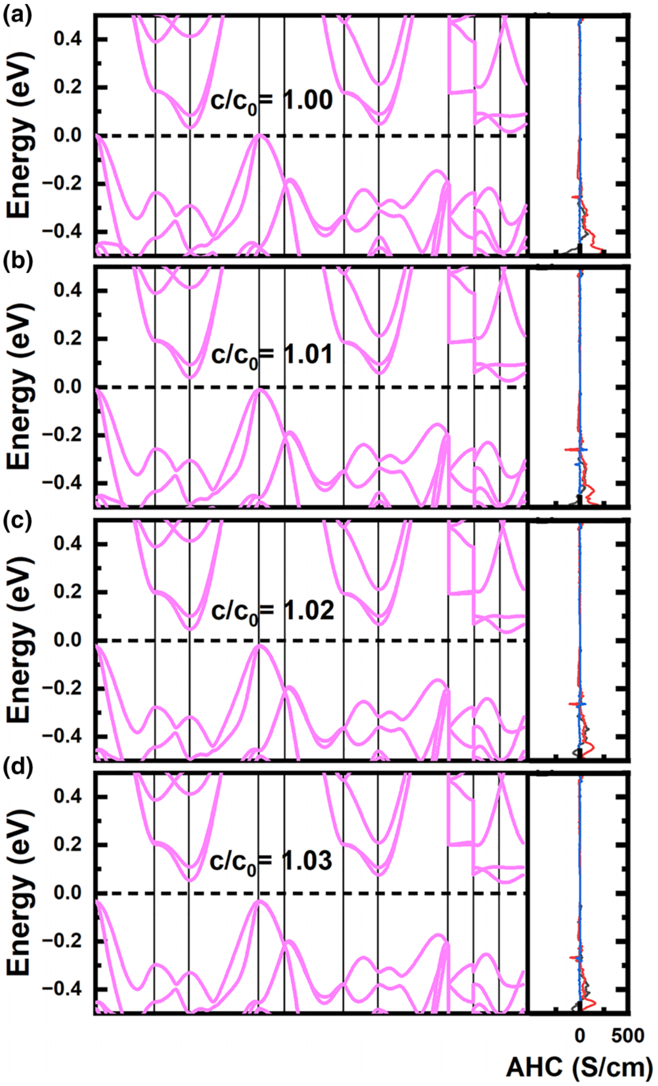

FIG. 10. The AHC at different tensile strains along the c axis of bulk $Mn_3Si_2Te_6$, where c/c_0 represents the ratio between the strained lattice parameter c and the initial value.

σ_{yz} appear in the broad energy region apart from the Fermi energy (0.30–0.45 eV). Note that the component σ_{zx} vanishes identically due to the mirror symmetry $\mathcal{M}_{xz}$ [25,56].

VI. CONCLUSIONS

Based on systematic first-principles calculations and symmetry analysis, we predicted monolayer $Mn_3Si_2Te_6$ is a stable FM material with in-plane collinear magnetization and no imaginary phonon frequency. Meanwhile, a large sixfold IPAHE appears in monolayer $Mn_3Si_2Te_6$ and exhibits sign reversal by manipulating magnetization orientation due to its weak in-plane MAE. Additionally, moderate strains could effectively change the energy bands and noticeably affect the distribution of the AHE with regard to the Fermi energy. Thus, monolayer $Mn_3Si_2Te_6$ provides an ideal platform for achieving the IPAHE and further investigating the interplay among magnetism, electronic topology, and exotic orbital physics.

ACKNOWLEDGMENTS

The authors acknowledge Jin Cao, Ruichun Xiao, Run Yang, and Zeying Zhang for useful discussions. This work was supported by the National Natural Science Foundation of China under Grants No. U2032164 and No. 12174394 and by the High Magnetic Field Laboratory of Anhui Province and the HFIPS Director's Fund (Grants No. YZJJQY202304 and No. BJPY2023B05) as well as by the Chinese Academy of Sciences under Contract No. JZHKYPT-2021-08.

APPENDIX A: COMPUTATIONAL DETAILS

All DFT [57,58] calculations with and without spin-orbit coupling (SOC) were performed with the Perdew-Burke-Ernzerhof exchange-correlation functional [59] using a plane-wave basis set and the projector-augmented wave method [60], as implemented in the Vienna Ab initio Simulation Package (VASP) [61]. A plane-wave basis set with a kinetic energy cutoff of 350 eV is considered while performing first-principles calculations. Furthermore, we have used a Γ-centered Monkhorst-Pack (7 × 7 × 1) k-point mesh for the BZ sampling and Gaussian smearing of 0.05 eV. Previous study has shown that the GGA itself provides excellent agreement with both the magnitude of the Curie temperature and the Curie-Weiss Θ obtained from the exchange constants [30], so the Hubbard U is not considered in our calculations. A 3 × 3 × 1 supercell with 3 × 3 × 1 k-mesh is used to obtain phonon dispersion via the density functional perturbation theory. The absence of imaginary phonon frequency suggests the dynamical stability of monolayer $Mn_3Si_2Te_6$, as shown in Fig. 5. To explore the nontrivial band topology and the intrinsic AHE, the tight-binding Hamiltonian was constructed with the maximally localized Wannier functions [62–64] to reproduce closely the band structure including SOC within ±1 eV of the E_F with Mn s-d, Si s-p, and Te p orbitals.

APPENDIX B: MAGNETIC GROUND STATE

To obtain the magnetic ground state of monolayer $Mn_3Si_2Te_6$, we considered a ferromagnetic configuration and three antiferromagnetic configurations with x, y, and z directions, respectively, as shown in Fig. 6. These calculated energies relative to the ferromagnetic ground state are listed in Table III. From the calculations, magnetization prefers to lie in basal plane. Because of the tiny difference between spin x and spin y, detailed calculations are needed to explore the in-plane magnetic anistropic energy (see Fig. 1 in the main text).

---

[1] N. Nagaosa, J. Sinova, S. Onoda, A. H. MacDonald, and N. P. Ong, Rev. Mod. Phys. **82**, 1539 (2010).

[2] D. Xiao, M.-C. Chang, and Q. Niu, Rev. Mod. Phys. **82**, 1959 (2010).

[3] X. Lin, W. Yang, K. L. Wang, and W. Zhao, Nat. Electron. **2**, 274 (2019).

[4] H. Polshyn, J. Zhu, M. A. Kumar, Y. Zhang, F. Yang, C. L. Tschirhart, M. Serlin, K. Watanabe, T. Taniguchi, A. H. MacDonald, and A. F. Young, Nature (London) **588**, 66 (2020).

[5] Z. Wang, H. Wu, G. W. Burr, C. S. Hwang, K. L. Wang, Q. Xia, and J. J. Yang, Nat. Rev. Mater. **5**, 173 (2020).

[6] T. Cao, D.-F. Shao, K. Huang, G. Gurung, and E. Y. Tsymbal, Nano Lett. **23**, 3781 (2023).

[7] L. D. Landau, L. P. Pitaevskii, and E. Lifshitz, *Electrodynamics of Continuous Media*, 2nd ed. (Butterworth-Heinemann, London, 1984).

[8] A. Pippard, *Magnetoresistance in Metals* (Cambridge University, Cambridge, England, 1989).

[9] A. A. Taskin, H. F. Legg, F. Yang, S. Sasaki, Y. Kanai, K. Matsumoto, A. Rosch, and Y. Ando, Nat. Commun. **8**, 1340 (2017).

[10] G. Yin, J.-X. Yu, Y. Liu, R. K. Lake, J. Zang, and K. L. Wang, Phys. Rev. Lett. **122**, 106602 (2019).

[11] L. Li, J. Cao, C. Cui, Z.-M. Yu, and Y. Yao, Phys. Rev. B **108**, 085120 (2023).

[12] J. Zhong, J. Zhuang, and Y. Du, Chin. Phys. B **32**, 047203 (2023).

[13] Y. Zhang and C. Zhang, Phys. Rev. B **84**, 085123 (2011).

[14] X. Liu, H.-C. Hsu, and C.-X. Liu, Phys. Rev. Lett. **111**, 086802 (2013).

[15] Y. Ren, J. Zeng, X. Deng, F. Yang, H. Pan, and Z. Qiao, Phys. Rev. B **94**, 085411 (2016).

[16] P. Zhong, Y. Ren, Y. Han, L. Zhang, and Z. Qiao, Phys. Rev. B **96**, 241103(R) (2017).

[17] X.-L. Sheng and B. K. Nikolić, Phys. Rev. B **95**, 201402 (2017).

[18] Z. Liu, G. Zhao, B. Liu, Z. F. Wang, J. Yang, and F. Liu, Phys. Rev. Lett. **121**, 246401 (2018).

[19] J.-Y. You, C. Chen, Z. Zhang, X.-L. Sheng, S. A. Yang, and G. Su, Phys. Rev. B **100**, 064408 (2019).

[20] J. Zhang, Z. Liu, and J. Wang, Phys. Rev. B **100**, 165117 (2019).

[21] H. Tan, Y. Liu, and B. Yan, Phys. Rev. B **103**, 214438 (2021).

[22] J. H. Cullen, P. Bhalla, E. Marcellina, A. R. Hamilton, and D. Culcer, Phys. Rev. Lett. **126**, 256601 (2021).

[23] S. Sun, H. Weng, and X. Dai, Phys. Rev. B **106**, L241105 (2022).

[24] Z. Li, Y. Han, and Z. Qiao, Phys. Rev. Lett. **129**, 036801 (2022).

[25] J. Cao, W. Jiang, X.-P. Li, D. Tu, J. Zhou, J. Zhou, and Y. Yao, Phys. Rev. Lett. **130**, 166702 (2023).

[26] J. Zhou, W. Zhang, Y.-C. Lin, J. Cao, Y. Zhou, W. Jiang, H. Du, B. Tang, J. Shi, B. Jiang, X. Cao, B. Lin, Q. Fu, C. Zhu, W. Guo, Y. Huang, Y. Yao, S. S. P. Parkin, J. Zhou, Y. Gao *et al.*, Nature (London) **609**, 46 (2022).

[27] J. Seo, C. De, H. Ha, J. E. Lee, S. Park, J. Park, Y. Skourski, E. S. Choi, B. Kim, G. Y. Cho, H. W. Yeom, S.-W. Cheong, J. H. Kim, B.-J. Yang, K. Kim, and J. S. Kim, Nature (London) **599**, 576 (2021).

[28] Y. Ni, H. Zhao, Y. Zhang, B. Hu, I. Kimchi, and G. Cao, Phys. Rev. B **103**, L161105 (2021).

[29] Y. Zhang, Y. Ni, H. Zhao, S. Hakani, F. Ye, L. DeLong, I. Kimchi, and G. Cao, Nature (London) **611**, 467 (2022).

[30] A. F. May, Y. Liu, S. Calder, D. S. Parker, T. Pandey, E. Cakmak, H. Cao, J. Yan, and M. A. McGuire, Phys. Rev. B **95**, 174440 (2017).

[31] Y. Liu and C. Petrovic, Phys. Rev. B **98**, 064423 (2018).

[32] L. M. Martinez, H. Iturriaga, R. Olmos, L. Shao, Y. Liu, T. T. Mai, C. Petrovic, A. R. Hight Walker, and S. R. Singamaneni, Appl. Phys. Lett. **116**, 172404 (2020).

[33] Y. Liu, Z. Hu, M. Abeykoon, E. Stavitski, K. Attenkofer, E. D. Bauer, and C. Petrovic, Phys. Rev. B **103**, 245122 (2021).

[34] J. Wang, S. Wang, X. He, Y. Zhou, C. An, M. Zhang, Y. Zhou, Y. Han, X. Chen, J. Zhou, and Z. Yang, Phys. Rev. B **106**, 045106 (2022).

[35] F. Ye, M. Matsuda, Z. Morgan, T. Sherline, Y. Ni, H. Zhao, and G. Cao, Phys. Rev. B **106**, L180402 (2022).

[36] G. Sala, J. Y. Y. Lin, A. M. Samarakoon, D. S. Parker, A. F. May, and M. B. Stone, Phys. Rev. B **105**, 214405 (2022).

[37] S. Djurdjić Mijin, A. Šolajić, J. Pešić, Y. Liu, C. Petrovic, M. Bockstedte, A. Bonanni, Z. V. Popović, and N. Lazarević, Phys. Rev. B **107**, 054309 (2023).

[38] Y. Zhang, L.-F. Lin, A. Moreo, and E. Dagotto, Phys. Rev. B **107**, 054430 (2023).

[39] C. Ran, X. Mi, J. Shen, H. Wang, K. Yang, Y. Liu, G. Wang, G. Wang, Y. Shi, A. Wang, Y. Chai, X. Yang, M. He, X. Tong, and X. Zhou, Phys. Rev. B **108**, 125103 (2023).

[40] F. Xue, Y. Hou, Z. Wang, Z. Xu, K. He, R. Wu, Y. Xu, and W. Duan, Natl. Sci. Rev. **11**, nwad151 (2023).

[41] R. Olmos, P.-H. Chang, P. Mishra, R. R. Zope, T. Baruah, C. Petrovic, Y. Liu, and S. R. Singamaneni, J. Phys. Chem. C **127**, 10324 (2023).

[42] Y. Lu, Z. Zhou, X. Kan, Z. Yang, H. Deng, B. Liu, T. Wang, F. Liu, X. Liu, S. Zhu, Q. Yu, and J. Wu, Nanomaterials **13**, 602 (2023).

[43] R. Rimet, C. Schlenker, and H. Vincent, J. Magn. Magn. Mater. **25**, 7 (1981).

[44] M. S. Dresselhaus, G. Dresselhaus, and A. Jorio, *Group Theory: Application to the Physics of Condensed Matter* (Springer Science & Business Media, Berlin, 2007).

[45] C.-C. Liu, W. Feng, and Y. Yao, Phys. Rev. Lett. **107**, 076802 (2011).

[46] P. Bampoulis, C. Castenmiller, D. J. Klaassen, J. van Mil, Y. Liu, C.-C. Liu, Y. Yao, M. Ezawa, A. N. Rudenko, and H. J. W. Zandvliet, Phys. Rev. Lett. **130**, 196401 (2023).

[47] D. Zhang, A. Rahman, W. Qin, X. Li, P. Cui, Z. Zhang, and Z. Zhang, Phys. Rev. B **101**, 205119 (2020).

[48] Spin-up means that the spin direction is the same as the direction of magnetization, while spin-down means that the spin direction is the opposite direction of of magnetization.

[49] H. Grimmer, Acta Crystallogr., Sect. A **49**, 763 (1993).

[50] M. Seemann, D. Ködderitzsch, S. Wimmer, and H. Ebert, Phys. Rev. B **92**, 155138 (2015).

[51] Due to the inaccuracy of numerical integrals, the AHC do not equal to 0 strictly at some special energy.

[52] F. D. M. Haldane, Phys. Rev. Lett. **61**, 2015 (1988).

[53] I. Sodemann and L. Fu, Phys. Rev. Lett. **115**, 216806 (2015).

[54] C. Ortix, Adv. Quantum Technol. **4**, 2100056 (2021).

[55] Z. Z. Du, C. M. Wang, H.-P. Sun, H.-Z. Lu, and X. C. Xie, Nat. Commun. **12**, 5038 (2021).

[56] T. Kurumaji, Phys. Rev. Res. **5**, 023138 (2023).

[57] W. Kohn and L. J. Sham, Phys. Rev. **140**, A1133 (1965).

[58] P. Hohenberg and W. Kohn, Phys. Rev. **136**, B864 (1964).

[59] J. P. Perdew, K. Burke, and M. Ernzerhof, Phys. Rev. Lett. **77**, 3865 (1996).

[60] P. E. Blöchl, Phys. Rev. B **50**, 17953 (1994).

[61] G. Kresse and J. Furthmüller, Phys. Rev. B **54**, 11169 (1996).

[62] N. Marzari, A. A. Mostofi, J. R. Yates, I. Souza, and D. Vanderbilt, Rev. Mod. Phys. **84**, 1419 (2012).

[63] N. Marzari and D. Vanderbilt, Phys. Rev. B **56**, 12847 (1997).

[64] I. Souza, N. Marzari, and D. Vanderbilt, Phys. Rev. B **65**, 035109 (2001).